Cancer Science

WILEY

Cancer Science

ORIGINAL ARTICLE OPEN ACCESS

Development of a Synthetic Lethality-Based Combination Therapy Using LIG1 and PARP Inhibitors for Prostate Cancer

Masaru Tani[1] | Koji Hatano[1] | Yu Ishizuya[1] | Toshiki Oka[1] | Tomohiro Kanaki[1] | Shunsuke Inoguchi[1] | Akihiro Yoshimura[1] | Yuki Horibe[1] | Yutong Liu[1] | Sassi Nesrine[1] | Yohei Okuda[1] | Akinaru Yamamoto[1] | Toshihiro Uemura[1] | Gaku Yamamichi[1] | Takuji Hayashi[1] | Yoshiyuki Yamamoto[1] | Taigo Kato[1] | Atsunari Kawashima[1] | Takao Yamaguchi[2] | Satoshi Obika[2] | Kosuke Yusa[3] | Norio Nonomura[1] | Keisuke Nimura[4]

[1]Department of Urology, The University of Osaka Graduate School of Medicine, Suita, Japan | [2]Graduate School of Pharmaceutical Sciences, The University of Osaka, Suita, Japan | [3]Stem Cell Genetics, Institute for Frontier Life and Medical Sciences, Kyoto University, Kyoto, Japan | [4]Division of Gene Therapy Science, Gunma University Initiative for Advanced Research, Gunma University, Maebashi, Japan

Correspondence: Koji Hatano (hatano@uro.med.osaka-u.ac.jp) | Keisuke Nimura (nimura@gunma-u.ac.jp)

Received: 1 April 2025 | **Revised:** 21 August 2025 | **Accepted:** 3 September 2025

Funding: This study was supported by the Japan Society for the Promotion of Science under KAKENHI (grant numbers 19K18610, 21K09345, and 24K12482).

Keywords: CRISPR-Cas9 knockout screening | LIG1 inhibitors | PARP inhibitor | prostate cancer | synthetic lethality

ABSTRACT

Despite advances in androgen receptor signaling inhibitors (ARSIs) and poly (ADP-ribose) polymerase inhibitors (PARPIs), metastatic castration-resistant prostate cancer (mCRPC) remains lethal. PARPIs clinical efficacy is limited in patients with homologous recombination repair deficiencies, such as *BRCA1/2* mutations, due to resistance. Thus, identifying novel synthetic lethal interactions with PARP may expand treatment options and improve therapeutic efficacy. Here, to identify genes that influence sensitivity to the PARPI olaparib, we conducted a genome-wide CRISPR-Cas9 knockout screening of 18,010 genes in DU145, 22Rv1, and LNCaP prostate cancer cell lines. Our screening identified PARP and LIG1 as synthetic lethality-inducing factors, whereas TP53 conferred resistance to PARPIs. Simultaneous inhibition of LIG1 and PARP increased DNA damage and apoptosis. Additionally, the combination of the LIG1 inhibitor L82-G17 with olaparib exhibited synergistic effects. To the best of our knowledge, we validated this combination therapy in vivo for the first time, suppressing tumor growth in a DU145 xenograft model while minimizing toxicity in normal tissues. Immunohistochemical analysis revealed that LIG1 was overexpressed in CRPC tissues, suggesting its potential as a therapeutic target. This study established LIG1 as a novel synthetic lethality-inducing factor in prostate cancer, showing that L82-G17 enhances the efficacy of olaparib, regardless of the *BRCA* mutation status. These findings suggest that the combination of PARP and LIG1 inhibitors could be a novel therapeutic strategy for mCRPC.

Abbreviations: ARSI, androgen receptor signaling inhibitor; CRPC, castration-resistant prostate cancer; DDR, DNA damage response; HRR, homologous recombination repair; PARPIs, poly (ADP-ribose) polymerase inhibitors.

Masaru Tani and Koji Hatano contributed equally.

1 | Introduction

Metastatic castration-resistant prostate cancer (mCRPC) remains lethal despite next-generation androgen receptor signaling inhibitors (ARSIs) and therapeutic advances [1]; changes in the DNA damage response (DDR) pathway are crucial for its aggressiveness [2]. Genomic analyses indicate that 20%–30% of patients with mCRPC harbor mutations in DDR-related genes, particularly in *BRCA1/2*, *ATM*, *CHEK2*, and *CDK12*, which are strongly associated with increased tumor aggressiveness and resistance [3–6]. Targeting these changes in the DDR pathway is a promising therapy for mCRPC.

Among the DDR-targeting approaches, poly (ADP-ribose) polymerase (PARP) inhibitors (PARPIs) are promising treatments for tumors with homologous recombination repair (HRR) deficiencies [7]. By inhibiting PARP1/2, PARPIs block the repair of single-strand breaks, leading to their accumulation and inducing synthetic lethality in HRR-deficient tumor cells [8, 9] Olaparib and rucaparib are FDA-approved PARPIs with clinical efficacy for treating patients with mCRPC *BRCA1/2* mutations [10–14]. However, their effectiveness in patients with non-BRCA DDR mutations or without HRR deficiencies is misunderstood, making mCRPC management challenging. Because the prognosis of patients with CRPC improves by combining PARPIs and ARSIs, the existence of unknown genes exhibiting synthetic lethality is possible [10, 15, 16].

PARPIs resistance is often driven by mechanisms such as HRR restoration or alternative repair pathways. To address this, the synergy of other DDR inhibitors, such as ATR or DNA-PK inhibitors, has been studied [17–20]. Beyond resistance management, expanding the indications of PARPIs requires novel synthetic lethal interactions and molecular targets.

Functional screens such as those using CRISPR identify targets of PARPIs sensitizers [17]. Using an sgRNA library, CRISPR screens targeting 356 DNA repair genesit was found that losing *LIG1*, *EMR1*, and *FAAP224* increased PARPIs efficacy [21]. However, the effects of these inhibitors have not been demonstrated in vivo.

Therefore, this study aimed to identify novel synthetic lethal genes associated with PARP in prostate cancer through genome-wide CRISPR screens targeting 18,010 genes, establishing a novel combination therapy to enhance PARPIs efficacy. We identified LIG1 as the most potent target for inducing synthetic lethality with a PARPI. We assessed LIG1 expression in clinical prostate cancer samples, including those from CRPC tissues. Our results indicate that LIG inhibitors have therapeutic effects in vivo.

2 | Materials and Methods

2.1 | Cell Culture

DU145, 22Rv1, and LNCaP prostate cancer cells were purchased from ATCC (Manassas, VA, USA) and maintained in basal media (DMEM for DU145 and RPMI1640 for 22Rv1 and LNCaP) supplemented with 10% fetal bovine serum in a humidified incubator set to 37°C and 5% CO_2.

2.2 | Lentivirus Packaging

Lentivirus packaging for gene transfer was performed using the Invitrogen ViraPower Lentiviral Packaging Mix (K497500; ThermoFisher Scientific, Waltham, MA, USA) following the manufacturer's protocol. Briefly, the vector plasmid and ViraPower Lentiviral Packaging Mix were transfected into HEK293FT cells using Lipofectamine 2000 (11668019; ThermoFisher Scientific, Waltham, MA, USA). The culture medium was changed after 24 h, and the cells were incubated for another 48 h. The culture supernatant containing the lentivirus was collected and stored at −80°C until use.

2.3 | Establishment of Cas9-Stably Expressing Prostate Cancer Cell Lines

Lentiviral supernatant prepared with Lenti-Cas9 blast (Addgene #52962) was added to DU145, 22Rv1, and LNCaP cells. The medium was replaced with fresh medium at 24 h. Cell selection was performed using blasticidin (DU145: 1.5 μg/mL, 22Rv1: 1.5 μg/mL, LNCaP: 1.5 μg/mL). The surviving cells were clonally isolated using the limiting dilution method.

2.4 | Cas9 Functional Assay

Cas9 function in cloned Cas9-expressing prostate cancer cells was assessed using a previously reported assay [22]. Briefly, gRNA against the green fluorescent protein (GFP), along with the coding sequences of blue fluorescent protein (BFP) and GFP mediated by the 2A-sequence, were introduced into cells using the lentiviral vector pKLV2-U6gRNA5(gGFP)-PGKBFP2AGFP-W (Addgene #67980). The cells were cultured for 5 days after transduction, and the expression of BFP and GFP was evaluated by flow cytometry, wherein the percentage of BFP-positive and GFP-negative cells determined Cas9 function, as GFP was knocked out. As a control, the same experiment was performed using pKLV2-U6gRNA5(Empty)-PGKBFP2AGFP-W (Addgene #67979), which does not express the gRNA for GFP, and it was confirmed that Cas9-expressing cells also became BFP- and GFP-positive cells. The clones with the highest Cas9 knockout efficiency in each prostate cancer cell line were used for CRISPR screening.

2.5 | gRNA Library

We used the Human Improved Genome-wide Knockout CRISPR Library v1, containing 90,709 gRNAs targeting 18,010 genes, which was gifted by Kosuke Yusa (Addgene #67989) [22].

2.6 | Generation of Genome-Wide Mutant Cell Pool and Screening

Overall, 3.0×10^7 Cas9-stably expressing prostate cancer cells (DU145, 22Rv1, and LNCaP) were transduced with a genome-wide gRNA lentiviral supernatant set to multiplicity of infection = 0.3. Two days after transduction, a proportion of the cells

was collected, and the percentage of gRNA-transfected cells that were BFP positive was 25%–35% by flow cytometry. Cell selection was performed using puromycin for 6 days. Genome-wide mutant cell pools obtained by cell selection were cultured for 14 days with olaparib and DMSO, the solvent for olaparib, as a control. These experiments started with 1.0×10^7 cells to obtain 100 cells per gRNA, and 1.0×10^7 cells were seeded during cell passages. Olaparib concentration was 2.5 μmol/L, which has negligible effect on proliferation in parent prostate cancer cells. After 14 days of culture, viable cells were collected, and genomic DNA was extracted from 5×10^6 olaparib-treated cells and 1.5×10^7 control olaparib-untreated cells using the DNeasy Blood and Tissue Kit (69504; Qiagen, Hilden, Germany). CRISPR screening was performed in three independent experiments for each cell line.

2.7 | gRNA Sequencing

Adapter and barcode sequences for sample discrimination were added to gRNA regions in genomic DNA extracted from cells by PCR, and the resulting PCR products were cleaned using the AMPure XP kit (A63881; Beckman Coulter, Brea, USA). Sequence library quality checks were performed using the TapeStation High Sensitivity D1000 (Agilent Technologies, Santa Clara, CA, USA). Genomic RNA was sequenced using an Illumina sequencer. The enrichment and dropout of the guides and genes were analyzed using MAGeCK [23].

2.8 | MTS Cell Viability Assay

Cells were seeded in 96-well plates (DU145: 1.5×10^3 cells/100 μL, LNCaP: 3.0×10^3 cells/100 μL, and 22Rv1: 8.0×10^3 cells/100 μL) and incubated for 24 h. PARPIs and solvents were added to reach the previously described concentrations, and cells were cultured for another 72 h. Then, 20 μL of CellTiter 96 AQueous One Solution Reagent (G3580; Promega, Wisconsin, USA) was added and incubated at 37°C and 5% CO_2 for 1 h. Absorbance was measured at 490 nm using a microplate reader (Bio-Rad).

2.9 | SDS-PAGE and Western Blotting

Nucleoproteins from the cells were separated using 10% sodium dodecyl sulfate-polyacrylamide gel electrophoresis and transferred to polyvinylidene difluoride (PVDF, 22860; ThermoFisher Scientific, Waltham, MA, USA) membranes using a semidry transfer system (ThermoFisher Scientific). The membranes were probed with specific antibodies as indicated and incubated with horseradish peroxidase-conjugated secondary antibodies against mouse or rabbit immunoglobulin (1:5000, #7074; Cell Signaling Technology [CST], Beverly, MA, USA), followed by detection with enhanced chemiluminescence western blotting detection reagents (#07880, #02230, and #11644; Nacalai Tesque, Kyoto, Japan). The chemiluminescence detector was a ChemiDoc XRS Plus system (Bio-Rad). LIG1 (1:1000, EPR12464; Abcam, Cambridge, UK) and histone H3 (1:2000, 9717S; Cell Signaling Technology, Danvers, MA, USA) were used for immunological analysis.

2.10 | Neutral Comet Assay

DNA double-strand breaks were evaluated using a neutral comet assay [24]. Overall, 2×10^6 cells were seeded in six-well plates and cultured for 48 h with 20 μmol/L olaparib or DMSO. After collection, cells were adjusted to 2×10^6 cells/mL by adding phosphate buffered saline (PBS). Then, 15 μL of this cell suspension was mixed with 90 μL of 1% low melting point agarose and transferred onto the OxiSelect Comet assay slide (STA-353; Cell Biolabs Inc., San Diego, USA) and incubated for 30 min at 4°C. Cells were lysed in neutral buffer (1.2 M NaCl, 100 mM EDTA, 10 mM Tris, 1% sodium lauryl sarcosinate, 0.5% TritonX-100, and 10% dimethylsulfoxide at pH 9.5) for 2 h at 4°C and electrophoresed for 25 min in TBE buffer at 12 V and 4 mA constant current. The cells were stained with Vista Green DNA Dye (235003; Cell Biolabs Inc., San Diego, CA, USA). At least 50 cells were analyzed using OpenComet software [25].

2.11 | Annexin V/Propidium Iodide Apoptosis Assay

Non-target gRNA or LIG1 gRNA-transfected 22Rv1 cells were seeded in six-well plates (3×10^5 cells/well) and DMSO or olaparib (20 μM) was added. After 72 h of culture, cells were collected, stained with an Annexin V-FITC Apoptosis Staining/Detection Kit (ab14085; Abcam, Cambridge, UK), and detected by flow cytometry.

2.12 | Immunofluorescence

DU145 and 22Rv1 cells were seeded onto eight-well chamber slides (SCS-N18; Matsunami Glass Ind. Ltd., Osaka, Japan) at densities of 2×10^4 and 1×10^5 cells/1.5 mL/well, respectively, and incubated overnight. Drug treatment was performed the following day; after 48 h, the cells were washed with PBS and fixed with 4% paraformaldehyde on ice for 15 min. Permeabilization was performed using PBS containing 0.1% Triton X-100 (87361; Muto Pure Chemicals Co. Ltd.) for 15 min at room temperature. For immunostaining, primary antibodies were diluted in PBS-T and incubated overnight at 4°C. Rabbit anti-phospho-histone H2A.X monoclonal antibody (#9718; Cell Signaling Technology) was used at 1:400. After washing with PBS, the slides were incubated at room temperature for 30 min with Alexa Fluor 568 goat anti-rabbit IgG (ab175471; Abcam) diluted 1:500 in PBS-T. The slides were then washed with PBS-T and counterstained with the ProLong Gold Antifade reagent containing DAPI (P36931; Invitrogen). Fluorescence images were acquired using a fluorescence microscope (BZ-X710; KEYENCE). The extent of DNA damage was quantified by calculating the percentage of γH2AX-positive cells (cells with 10 RAD51 nuclear foci) relative to the total number of DAPI-stained cells.

2.13 | Drug Synergy Analysis

DU145 cells were seeded in a 96-well plate (1500 cells/well) and treated with DMSO or three doses of olaparib (1, 5, and 10 μM) and L82-G17 (1, 5, 10, 20, 40, 50, and 75 μM) in a

matrix format. After 5 days, the MTS cell viability assay was performed. Drug synergy scores were calculated based on the HSA model using SynergyFinder 3.0 (https://synergyfinder.fimm.fi/) [26].

2.14 | In Vivo Xenograft Studies

To establish a human prostate cancer xenograft model in immunodeficient mice (Icr-*scid/scid*Jcl obtained from CLEA Japan), DU145 cells (1×10^6 cells in 100 μL of culture medium) were injected into the right flank of 5-week-old male mice. Tumor growth was monitored regularly using a digital caliper, and tumor volume was calculated using the formula: $(\text{width})^2 \times \text{length}/2$. Once the tumor volume exceeded 200 mm^3, mice were randomly assigned to vehicle control ($n = 7$), olaparib ($n = 7$), L82-G17 ($n = 7$), or combination therapy ($n = 7$) groups. Vehicle, olaparib (50 mg/kg), and L82-G17 (50 mg/kg) were administered intraperitoneally twice a week (200 μL per injection). The mice were euthanized on day 30 post-treatment or earlier if the tumors reached the maximum ethical size. A portion of the harvested tumors was fixed in 10% neutral-buffered formalin. All animal procedures were approved by the Osaka University Animal Research Committee and conducted in accordance with the relevant regulatory standards.

2.15 | Immunofluorescence of Formalin-Fixed, Paraffin-Embedded (FFPE) Samples

FFPE subcutaneous tumor sections from mice were subjected to antigen retrieval using EDTA buffer (pH 9.0) and heated at 110°C for 4 min in a Pascal pressure chamber (S2800; Dako). The sections were then incubated in blocking buffer (DAKO wash buffer supplemented with 1% bovine serum albumin) for 5 min.

For immunostaining, primary antibody H2AX (1:400, #9718; Cell Signaling Technology [CST], Beverly, MA, USA) was diluted in DAKO Antibody Diluent and incubated at 4°C overnight. After washing, sections were incubated at room temperature for 30 min with the corresponding secondary antibody diluted in blocking buffer. Following washing with distilled water, the sections were mounted with ProLong Gold Antifade reagent containing DAPI (P36931; Invitrogen) and stored at 4°C. Fluorescence images were acquired using a fluorescence microscope (BZ-X710; KEYENCE). The extent of DNA damage was quantified by calculating the percentage of γH2AX-positive cells (cells with five RAD51 nuclear foci) relative to the total number of DAPI-stained cells.

2.16 | TUNEL Assay of FFPE Samples

TUNEL assay was performed on FFPE tissue sections using the TUNEL assay Kit (#25879; Cell Signaling Technology [CST], Beverly, MA, USA), according to the manufacturer's instructions. Tissue sections were deparaffinized, rehydrated, and treated with proteinase K (20 μg/mL) for 15 min at room temperature. After washing with PBS, sections were incubated with the TUNEL reaction mixture for 60 min at 37°C in a humidified chamber. Slides were then washed and counterstained with DAPI. Stained sections were mounted with antifade mounting medium and examined using a fluorescence microscope (BZ-X710; KEYENCE). TUNEL-positive nuclei were quantified as a percentage of total DAPI-stained nuclei.

2.17 | Immunohistochemical Studies

The immunohistochemical staining using human specimens was approved by the Ethics Committee of Osaka University, and we were allowed to omit the authorization and informed consent (No. 13397-23). Immunohistochemical staining was performed in 4 μm-thick paraffin-embedded tissue samples. Tumor sample sections were treated with EDTA buffer (pH 6.0) and activated by warming for 20 min for antigen activation. Endogenous peroxidase activity was blocked by incubating the sections with 0.3% hydrogen peroxide for 5 min, followed by overnight incubation at 4°C with primary antibodies against LIG1 (1:400, EPR12464; Abcam, Cambridge, UK), γH2AX (1:200, #9718; Cell Signaling Technology [CST], Beverly, MA, USA) and cleaved PARP (1:50, #5625; Cell Signaling Technology [CST], Beverly, MA, USA). Staining was performed using DAB substrate (MK210; TaKaRa, Shiga, Japan). The sections were counterstained with hematoxylin. For the immunohistochemical analysis of LIG1, the ratio of positive to tumor cells was counted in a 400× field of view, and the averages of the ratio were calculated using three different random fields per sample.

2.18 | Data Analysis and Statistics

Data are expressed as mean ± SE. If data followed a normal distribution in the Shapiro–Wilk test, comparisons were made with an unpaired *t*-test; if not, comparisons were made with a Mann–Whitney *U*-test. Statistical significance was set at $p < 0.05$. Analyses were performed using the JMP Pro 14 software (SAS Institute).

3 | Results

3.1 | Identification of Candidate Genes Affecting PARPI Sensitivity

To identify the genes influencing the sensitivity to PARPIs in prostate cancer cells, we performed genome-wide CRISPR knockout screening using DU145, 22Rv1, and LNCaP prostate cancer cell lines with stable Cas9 expression (Figure 1A). A genome-wide gRNA library targeting 18,010 genes was used to create a pool of cells with gene knockouts cultured for 14 days with olaparib or DMSO. Cells with knockouts of genes essential for survival under PARPIs were depleted, enabling the identification of candidate synthetic lethal genes through next-generation sequencing of gRNA in surviving cells.

Overall, 187, 204, and 231 negatively selected genes ($p < 0.01$) were identified in LNCaP, 22Rv1, and DU145 cells, respectively (Tables S1–S3), which enhanced olaparib sensitivity when

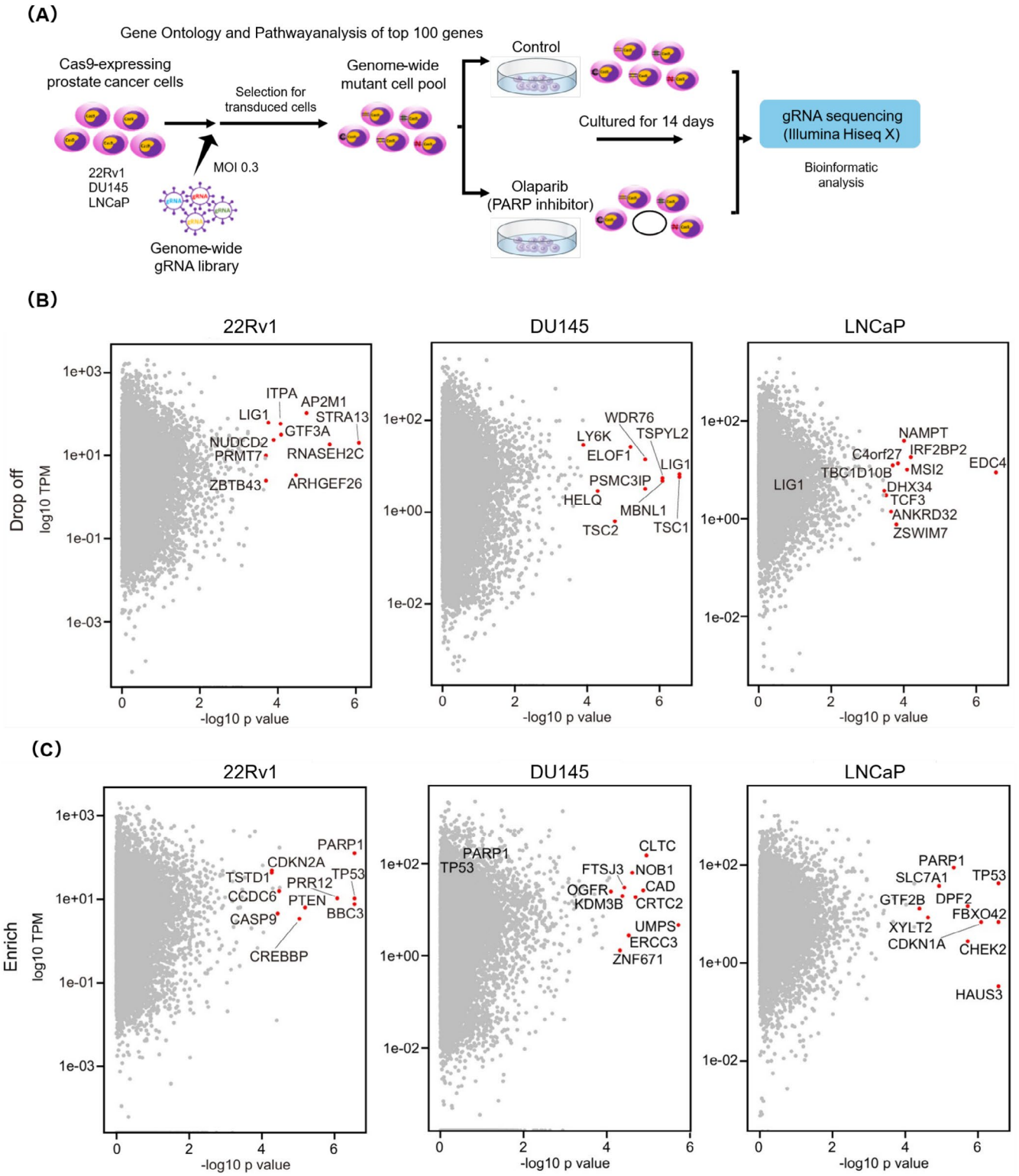

FIGURE 1 | Genome-wide CRISPR screening identifies synthetic lethal or resistant candidates with PARP inhibition in prostate cancer. (A) Genome-wide CRISPR-Cas9 knockout screen in DU145, 22Rv1, and LNCaP prostate cancer cell lines. Cells were transduced with a gRNA library targeting 18,010 genes and treated with olaparib or DMSO for 14 days before next-generation sequencing analysis. (B) Dot plots showing negatively selected genes following olaparib treatment indicate potential synthetic lethal interactions with PARPIs. The names of the top 10 genes are shown. (C) Dot plots displaying positively selected genes after olaparib treatment that suggest potential resistance mechanisms to PARPIs. The names of the top 10 genes are shown.

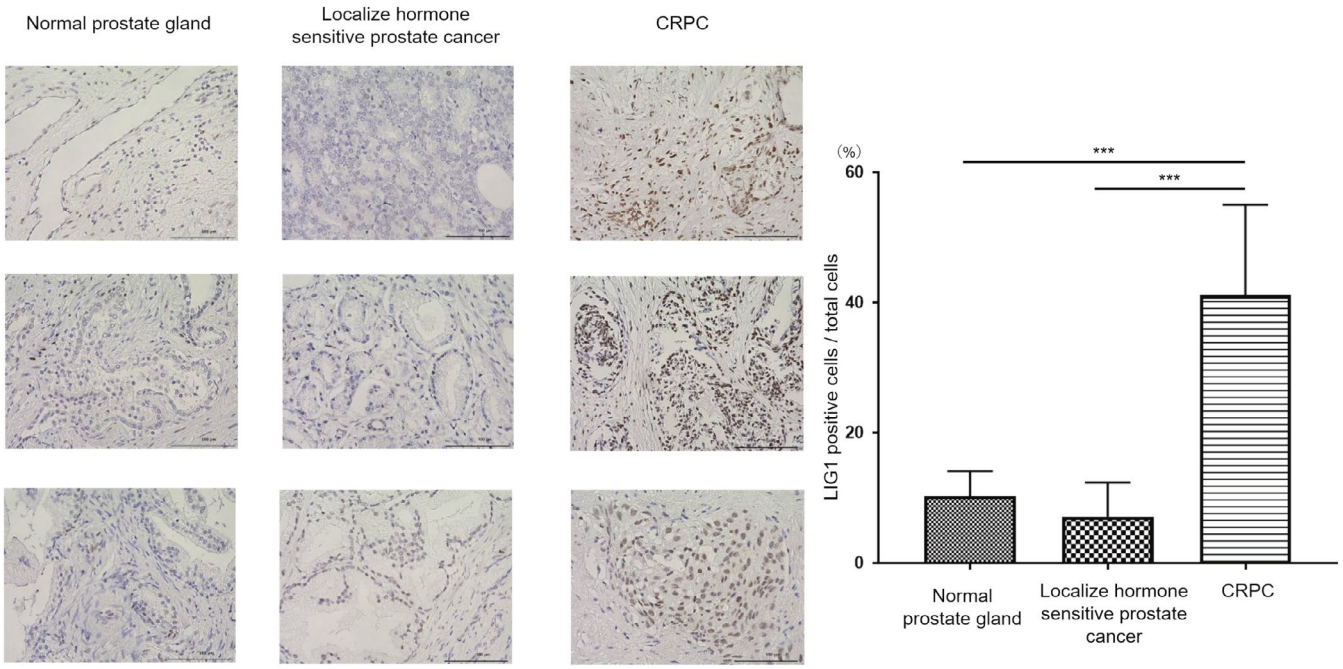

FIGURE 2 | Immunohistochemical analysis of LIG1 expression in human prostate tissues. Bar plot showing the percentage of LIG1 positive cells compared to that of the total cell population. Data are presented as mean ± SD ($n = 3$ biological replicates). p values were determined using the two-way ANOVA and Bonferroni's multiple comparisons test. ***$p < 0.001$.

knocked out (Figure 1B); 23 genes were identified in at least two cell lines. Gene Ontology (GO) analysis of genes downregulated under olaparib treatment revealed enriched pathways, such as DNA repair and replication, in DU145, 22Rv1, and LNCaP cells, confirming the relevance of these pathways to PARP function (Figure S1A). These results indicate that the screening approach was robust.

Additionally, 226, 224, and 278 positively selected genes that confer resistance to olaparib when knocked out ($p < 0.01$) were identified in LNCaP, 22Rv1, and DU145 cells, respectively (Tables S4–S6); 27 genes were identified in at least two cell lines (Figure 1C). PARP1 and PARP3 were common in both cell lines, and the knockout of the primary target of PARP inhibitors, PARP1, attenuated the effects of olaparib, supporting our experimental system (Figure S1B).

3.2 | LIG1 Enhances the PARPIs Efficacy in Prostate Cancer Cell Lines

As a promising candidate gene of synthetic lethality with PARP, we focused on LIG1, which ranked among the top 10 negatively selected genes under olaparib selection in 22Rv1 and DU145 cell lines. LIG1 is a member of the DNA ligase family crucial for DNA replication and single-strand break repair [27–29]. Increased LIG1 expression is detected in several cancers including breast, lung, colorectal, and ovarian [30]. Compared with normal prostate and localized hormone-sensitive prostate cancer tissues, we found that LIG1 was overexpressed in tissue samples from patients with CRPC (Figure 2). Additionally, TP53 and PARP1 were ranked in the top 10 of genes associated with olaparib resistance for LNCaP and 22Rv1 cell lines. Hence, we focused on TP53 as a promising candidate gene for olaparib resistance.

We validated LIG1 and TP53 functions in 22Rv1 and DU145 control and PARPIs knockout cells; *LIG1* knockdown did not affect cell proliferation (Figure S2). *LIG1* or *TP53* knockout cells (Figure 3A) were treated with the PARPIs olaparib or veliparib, and cell proliferation was assessed (Figure 3B). *TP53* knockout did not alter the sensitivity of TP53-mutant cells (DU145), while *TP53* knockout showed resistance of TP53-functional cells (22Rv1). *LIG1* knockout enhanced the sensitivity of DU145 and 22Rv1 cells to PARPIs (Figure 3B). We hypothesized that under *LIG1*-deficient conditions, PARPIs induce DNA damage and trigger cell death. Using a comet assay, we found that olaparib increased DNA breaks in *LIG1* knockout cells compared with those of control cells ($p < 0.001$) (Figure 4A). In DU145 cells treated with olaparib, the percentage of cells positive for γH2AX foci was higher in the LIG1 knockdown group than that of the control group (19.2 vs. 8.57%, $p = 0.022$) (Figure 4B). Using an Annexin V assay, we confirmed that olaparib induced apoptosis in *LIG1* knockout cells ($p < 0.05$) (Figure 4C). Therefore, *LIG1* deficiency enhances DNA damage and apoptosis following PARP inhibition, increasing the sensitivity of prostate cancer cells to PARPIs. Hence, LIG1 is a novel gene of synthetic lethality with PARP.

3.3 | LIG1 Inhibition Enhances the Therapeutic Effect of PARP Inhibition Through Synergistic Cytotoxicity

We evaluated the combination of LIG1 and PARP inhibition using the potent and selective LIG1 inhibitor L82-G17 [31, 32]. LNCaP, 22Rv1, and DU145 cells were treated with olaparib, L82-G17, or both. The combined treatment reduced cell viability in all cell lines compared to single treatments (Figure 5A). SynergyFinder was used to calculate synergy scores using the

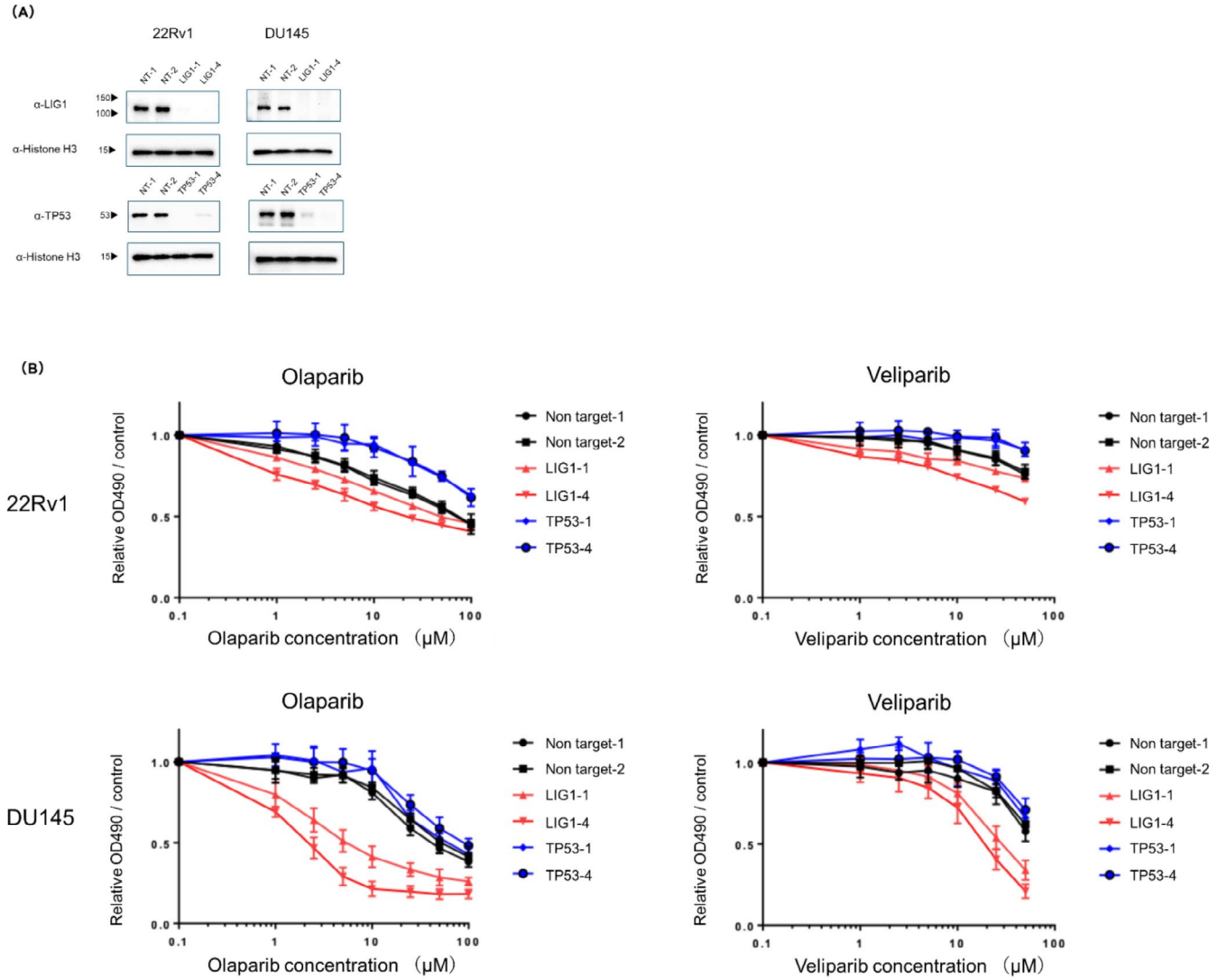

FIGURE 3 | Functional validation of LIG1 synthetic lethality with PARP and TP53 as resistance factors to PARPIs. (A) Western blot analysis of *LIG1* and *TP53* knockout efficiency in 22Rv1 and DU145 cells. (B) Cell viability assays of 22Rv1 and DU145 cells treated with olaparib or veliparib that evaluate the functional impact of LIG1 and TP53 knockouts on PARPIs sensitivity. This experiment was conducted using two independent clones for LIG1 and TP53 knockouts.

ZIP method, which revealed synergistic effects (most synergistic area score = 13.91) (Figure 5B).

Combination treatment enhanced γ-H2AX foci formation in 22Rv1 and DU145 cells compared with that of single-agent treatments, indicating increased DNA damage (DMSO: 5.4%, olaparib: 11.1%, L82-G17: 4.5%, and combination therapy: 23.4%) (Figure 5C). Thus, combined inhibition of LIG1 and PARP induced synergistic effects in prostate cancer cells.

3.4 | Combination Therapy Demonstrates Superior Antitumor Efficacy in DU145 Xenograft Models

The antitumor efficacy of combination therapy was evaluated in a DU145 xenograft mouse model (Figure 6A). No differences were observed in body weight among the control, olaparib monotherapy, L82-G17 monotherapy, and combination therapy groups, indicating minimal systemic toxicity (Figure 6B). Combining olaparib and L82-G17 suppressed tumor growth compared to the control and olaparib and L82-G17 monotherapy groups (Figure 6C). Immunohistochemical analysis of tumor tissues revealed increased γ-H2AX expression in the combination therapy group, supporting the induction of DNA damage (Figure 6D). The expression of cleaved PARP was also elevated in the combination group, supporting the induction of apoptosis (Figure 6E). Furthermore, the TUNEL assay revealed increased DNA fragmentation in the combination therapy group, reinforcing DNA damage as a key mechanism of action (Figure 6F). Hence, combining LIG1 and PARP inhibition exhibited synergistic cytotoxic effects in in vitro and in vivo prostate cancer models.

4 | Discussion

PARPIs are used to treat prostate cancer; however, their effectiveness is constrained by the limited patient population that

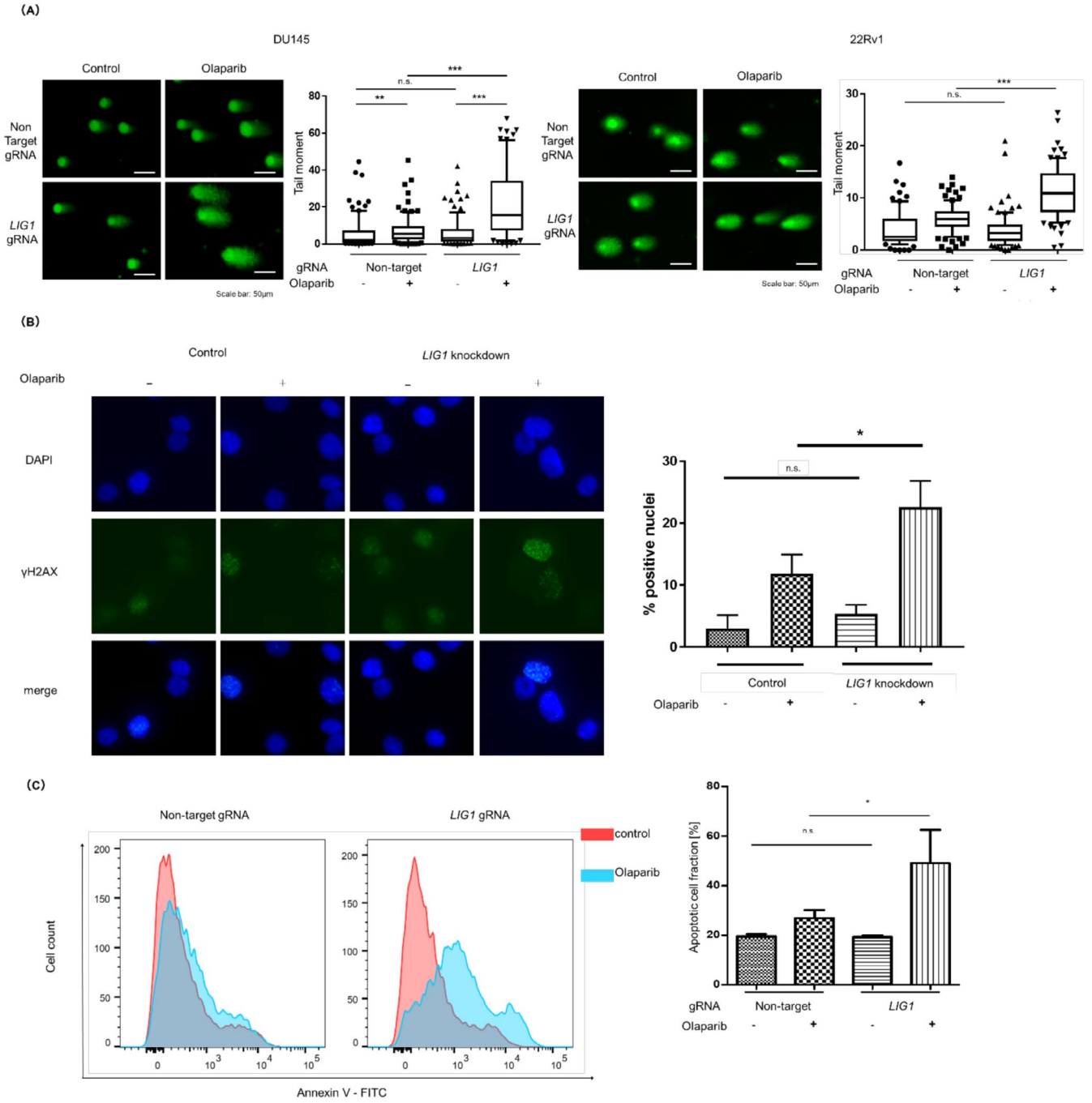

FIGURE 4 | LIG1 deficiency enhances DNA damage and apoptosis upon PARP inhibition. (A) Comet assay of DNA damage levels in LIG1 knockout and control 22Rv1 and DU145 cells following olaparib treatment. The comet tail moment was measured in the treated and untreated groups. The box plots represent the mean values for each condition. Data are presented as mean ± SD ($n = 3$ biological replicates). p values were determined using two-way ANOVA and Bonferroni's multiple comparison test. (B) Immunofluorescence analysis of γ-H2AX foci in DU145 cells to visualize DNA damage levels in LIG1 knockout versus control cells following olaparib treatment. Bar plot showing the percentage of cells with more than 10 γ-H2AX foci compared to that of the total cell population. Blue and green indicate DAPI and γ-H2AX staining, respectively. Data are presented as mean ± SD ($n = 3$ biological replicates). p values were determined using two-way ANOVA and Bonferroni's multiple comparison test for the control and *LIG1* knockdown samples. (C) Annexin V assessment of the induction in *LIG1* knockout and control cells following PARPI treatment. Flow cytometry showing differences apoptosis levels between control and *LIG1* knockout cells after treatment with olaparib. Red and blue indicate control and *LIG1* knockout cells, respectively. Bar plot showing the percentage of apoptotic cells per condition. Data are presented as mean ± SD ($n = 3$ biological replicates). p values were determined using two-way ANOVA and Bonferroni's multiple comparison test for control and sgLIG1 samples. Significance values: $^{*}p < 0.05$, $^{**}p < 0.01$, $^{***}p < 0.001$; n.s., not significant.

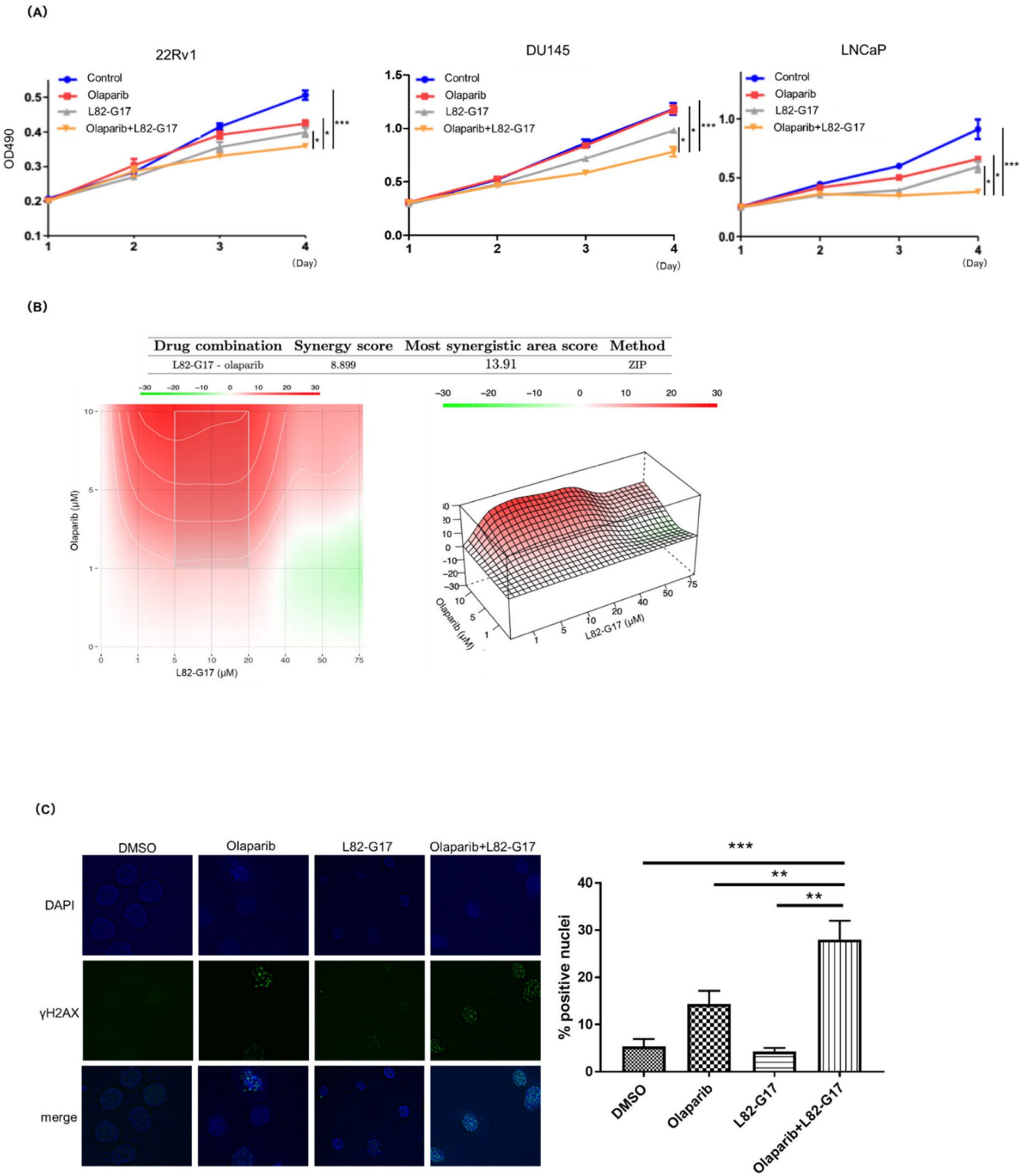

FIGURE 5 | Synergistic effects of the LIG1 inhibitor L82-G17 and olaparib therapy in prostate cancer cells. (A) Cell viability assays in prostate cancer cells treated with olaparib, L82-G17, or their combination. *p* values were determined using one-way ANOVA and Tukey's multiple comparison test. (B) Synergy analysis of olaparib and L82-G17 in DU145 cells using the ZIP model in SynergyFinder. (C) Immunofluorescence analysis of γ-H2AX foci formation in DU145 cells. Bar plot showing the percentage of cells with more than 10 γ-H2AX foci compared to that of the total cell population. Blue and green indicate DAPI and γ-H2AX staining, respectively. Data are presented as mean ± SD ($n = 3$ biological replicates). *p* values were determined using one-way ANOVA and Tukey's multiple comparison test. $^{*}p \leq 0.05$; $^{**}p \leq 0.01$; $^{***}p \leq 0.001$.

benefits from them and their relatively short duration of response [33, 34]. Recently, combining ARSIs and PARPIs has been shown effective [15, 16], prompting a shift toward these combinatorial approaches [33]. Nonetheless, several questions remain regarding optimal selection criteria and predictive markers for treatment efficacy. Although several studies have

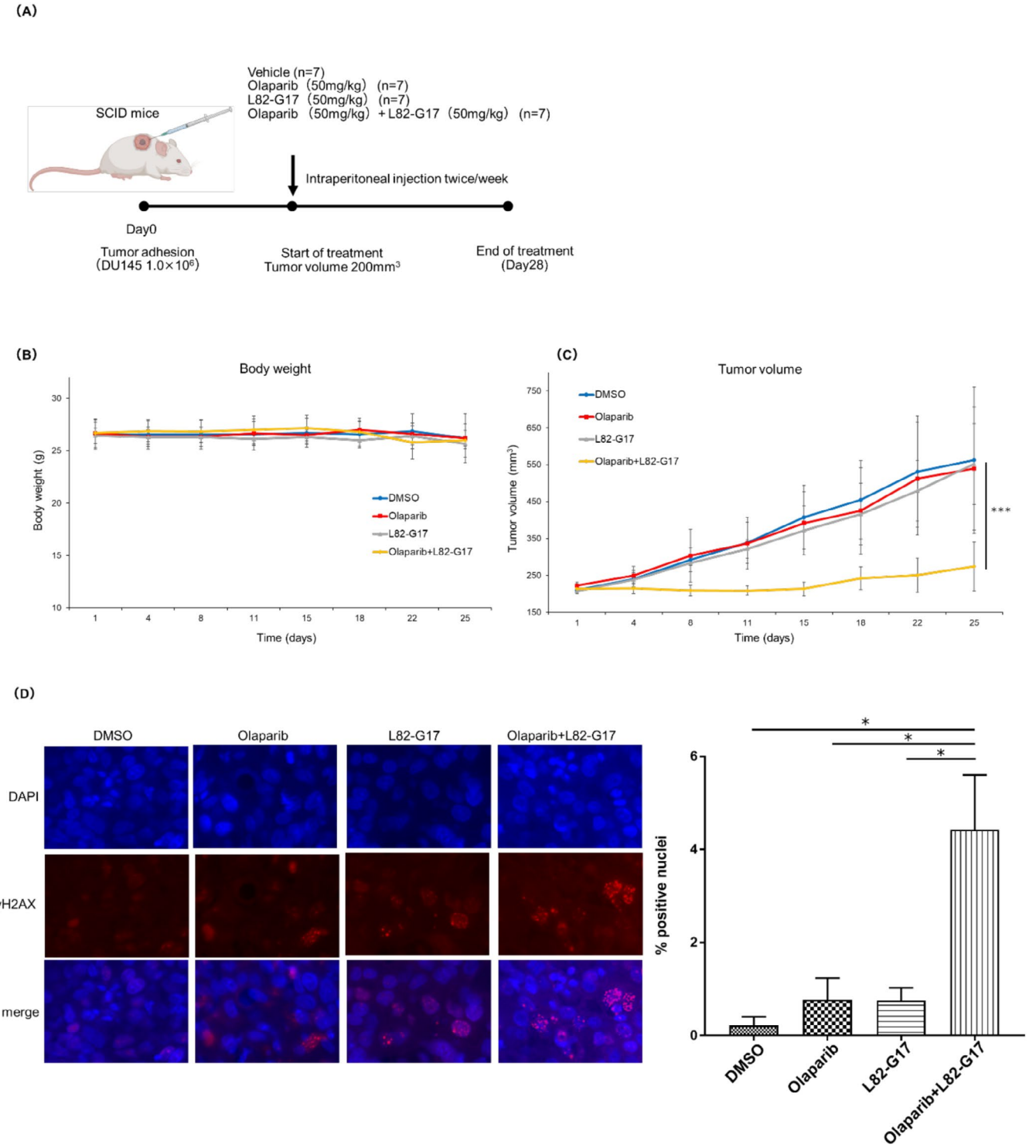

FIGURE 6 | In vivo efficacy of L82-G17 and olaparib therapy in a DU145 xenograft model. (A) Mice were randomized into DMSO (control), olaparib, L82-G17, and olaparib and L82-G17 groups. (B) Line graph showing the changes in the body weight of mice. (C) Line graph showing changes in tumor volume. (D) Immunofluorescence analysis of γ-H2AX foci formation in FFPE tumor samples. Blue and red indicate DAPI and γ-H2AX staining, respectively. Bar plot showing the percentage of cells with more than 5 γ-H2AX foci compared to that of the total cell population. (E) Immunohistochemical analysis of cleaved PARP expression in FFPE tumor samples. Representative images and bar plot showing the percentage of cleaved PARP-positive cells relative to the total cell population. (F) TUNEL assay in FFPE tumor samples. Blue and green indicate DAPI and TUNEL-positive nuclei, respectively. Bar plot showing the percentage of TUNEL-positive cells relative to the total cell population. Data are presented as mean ± SD. *p* values were determined using one-way ANOVA and Tukey's multiple comparison test. $*p \leq 0.05$, $**p < 0.01$, $***p < 0.001$.

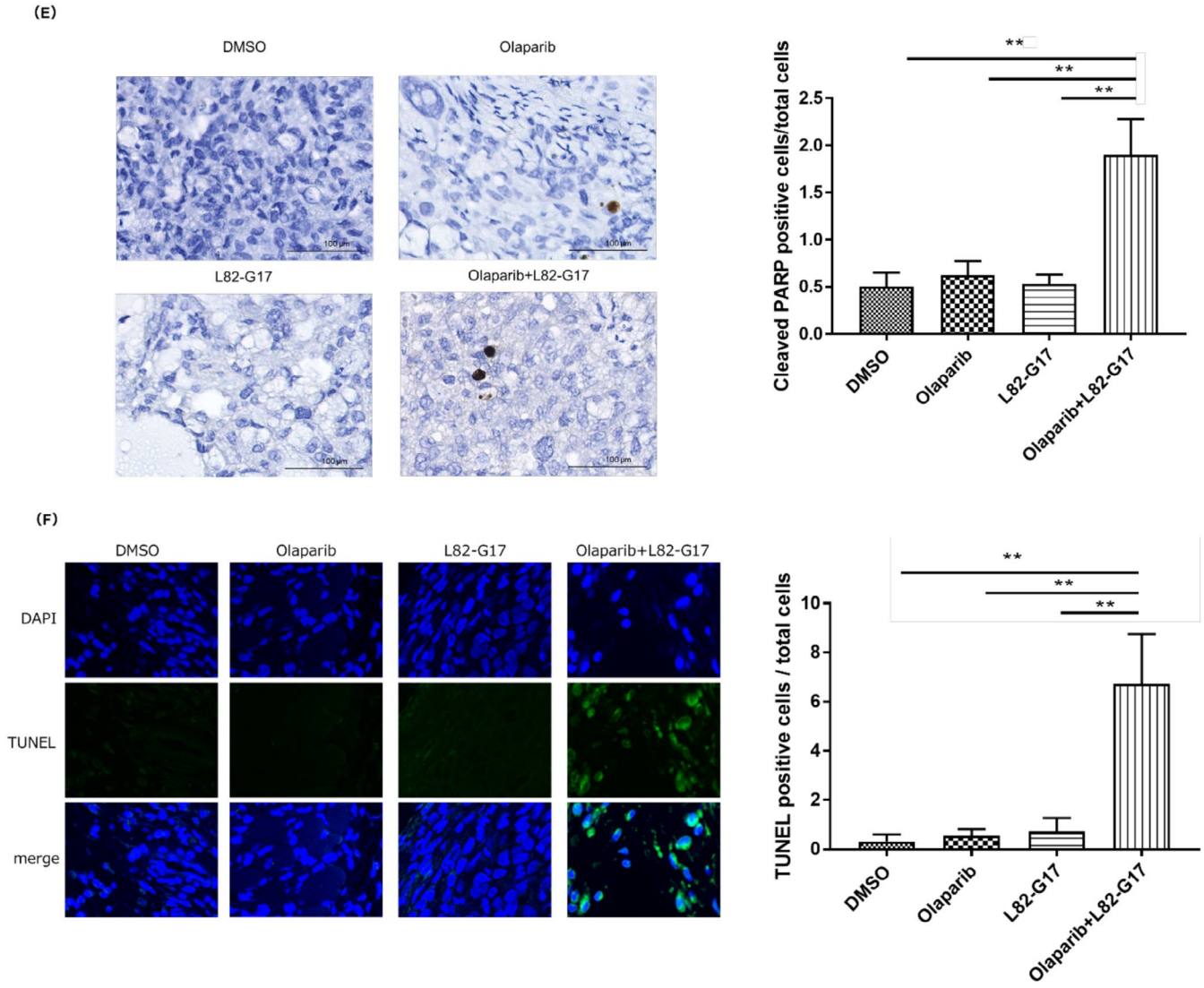

FIGURE 6 | (Continued)

identified genes of synthetic lethality with PARP [25–37], the number of drugs that have been successfully translated into clinically applied combination therapies with PARPIs remains limited.

We conducted a genome-wide CRISPR-Cas9 knockout screen using an 18,010-gene sgRNA library of prostate cancer cell lines with functional BRCA1/2 [17, 21, 38]. GO analysis of genes significantly reduced by PARPIs revealed that pathways related to DNA repair and replication are enriched in DU145 and 22Rv1 cells. From these genes, we focused on LIG1, involved in DNA repair pathways and ranked within the top 10 as a promising candidate exhibiting synthetic lethality with PARPIs. LIG1 is a key synthetic lethality partner of PARP according to studies using CRISPR screening in prostate cancer cells [17, 39, 40]. While concluding this study, Fracassi et al. reported LIG1 as a gene showing synthetic lethality with PARP using a custom sgRNA library of DNA damage repair genes, reporting the relationship between LIG1 and PARP [21]. We evaluated the combination of olaparib and L82-G17 in vivo and investigated LIG1 expression in human prostate tissues.

LIG1 is essential for DNA replication and base excision repair [41]; when lacking, a compensatory repair mechanism involving the LIG3-XRCC1 complex is activated, partially substituting LIG1 [42]. In *LIG1*-knockout prostate cancer cell lines, their viability is unaffected. Conversely, when LIG1-knockout prostate cancer cells were treated with olaparib, cell viability was significantly reduced. Additionally, when *LIG1*-knockout prostate cancer cell lines were treated with olaparib, DNA damage increased, and apoptosis was induced. When LIG1 is deficient, poly (ADP-ribose), crucial for recruiting the LIG3-XRCC1 complex to sites of DNA damage, is activated [43]. Increased PAR activity occurs because PARP1/2 recognizes the accumulating single-stranded breaks between unligated Okazaki fragments arising from LIG1 deficiency, promoting enhanced PAR synthesis at these sites [44–46]. Therefore, considering that LIG1 and PARP1/2 inhibition would show synthetic lethality when combined is reasonable.

Li et al. reported that CRPC cells show increased expression of several HRR-related genes. Among them, *LIG1* mRNA expression is higher in CRPC than that in normal prostate and localized

prostate cancer tissues [47], justifying LIG1 as a therapeutic target. The mutation frequency of *LIG1* is approximately 6% in TCGA datasets of CRPC [21], suggesting its value as a predictive biomarker of PARPIs efficacy. Immunohistochemistry confirmed that LIG1 was overexpressed in CRPC tissues compared with normal prostate and localized prostate cancer tissues. LIG1 overexpression is associated with tumor aggressiveness and poor prognosis in ovarian cancer [48]. Polymorphic variants of LIG1 may affect lung, upper gastrointestinal [49], and head and neck cancers [50]. These findings suggest that LIG1 inhibitors may exert selective toxicity in cancer cells while sparing normal cells. The toxicity of LIG1 inhibitors in normal prostate cells is reportedly lower than that in prostate cancer cell lines [21].

We tested a combination of LIG1 inhibitors and PARPIs. Through in silico structure-based screening of LIG1-nicked DNA complexes, small-molecule LIG1 inhibitors, including L82, L67, and L189, were identified [32]. Additionally, L82-G17 is a next-generation inhibitor with excellent selectivity and efficacy for LIG1 [31]. We found that L82-G17 had synergy with the PARP inhibitor olaparib, significantly reducing the viability of multiple prostate cancer cell lines. Conversely, L82, L67, and L189 showed no synergy with olaparib (data not shown), probably because L82-G17 is a non-competitive inhibitor of phosphate diester bond formation, which is the third stage of the DNA phosphorylation reaction; the accumulation of DNA adenylate intermediates may contribute to this [31]. The DNA structure wherein PARP is trapped is unknown; recently, it has been suggested that free Okazaki fragments are such structures [51]. Hence, the DNA adenylic acid intermediate accumulated by L82-G17 may enhance the ability of PARPIs to bind to DNA, enhancing their cytotoxicity through PARP trapping.

In this study, using prostate cancer cell lines with functional BRCA (22Rv1 and DU145 cells) [17, 21], we demonstrated that the novel mechanism of synthetic lethality induced by the combination of L82-G17 and olaparib is effective even in cells without BRCA mutations. This suggests that this combination therapy can broaden treatment options for patient populations previously limited to therapeutic alternatives. Ali et al. reported that HDR-deficient cells exhibited hypersensitivity to a LIG1 inhibitor [48], implying that L82-G17 might also be effective as a monotherapy in HDR-deficient cancers.

To the best of our knowledge, this is the first in vivo study of L82-G17 with olaparib. This combination enhanced the therapeutic efficacy compared to single treatments and did not result in weight loss in mice relative to that of the control or monotherapy groups, suggesting that it exerted a tumor-selective effect with minimal toxicity to normal tissues; this may be due to the higher expression of LIG1 in tumor tissues. The response to LIG1 and PARP inhibition differs among tumor types [21], with tissue-specific LIG1 expression levels potentially influencing therapeutic outcomes.

This study had limitations. We demonstrated the synergy of L82-G17 and olaparib in vitro in a DU145 xenograft model, but the long-term efficacy and potential emergence of resistance were not completely explored. The synergy mechanism, particularly PARP trapping and the compensatory activation of the LIG3-XRCC1 pathway, requires further investigation. Although our preliminary in vivo toxicity data are promising, off-target effects and systemic toxicity in normal tissues analyses are necessary before considering clinical applications. The number of human tissue samples for LIG1 immunostaining was small, which may restrict the generalizability of our findings regarding LIG1 expression in clinical samples.

In conclusion, LIG1 may increase PARPIs efficiency. The LIG1 inhibitor L82-G17 and olaparib showed synergistic effects in prostate cancer cells with or without BRCA mutations, potentially expanding treatment options for underserved patients.

Author Contributions

Masaru Tani: conceptualization, data curation, formal analysis, investigation, methodology, project administration, resources, validation, visualization, writing – original draft. **Koji Hatano:** conceptualization, data curation, formal analysis, funding acquisition, investigation, methodology, project administration, resources, validation, writing – original draft, writing – review and editing. **Yu Ishizuya:** conceptualization, data curation, investigation, methodology, resources, validation, writing – original draft. **Toshiki Oka:** investigation, methodology, resources, validation, writing – review and editing. **Tomohiro Kanaki:** investigation, methodology, resources, validation, writing – review and editing. **Shunsuke Inoguchi:** investigation, methodology, resources, validation, writing – review and editing. **Akihiro Yoshimura:** investigation, methodology, resources, validation, writing – review and editing. **Yuki Horibe:** investigation, methodology, resources, validation, writing – review and editing. **Yutong Liu:** investigation, methodology, resources, validation, writing – review and editing. **Sassi Nesrine:** investigation, methodology, resources, validation, writing – review and editing. **Yohei Okuda:** investigation, methodology, resources, validation, writing – review and editing. **Akinaru Yamamoto:** investigation, methodology, resources, validation, writing – review and editing. **Toshihiro Uemura:** investigation, methodology, resources, validation, writing – review and editing. **Gaku Yamamichi:** investigation, methodology, resources, validation, writing – review and editing. **Takuji Hayashi:** investigation, methodology, resources, validation, writing – review and editing. **Yoshiyuki Yamamoto:** investigation, methodology, resources, validation, writing – review and editing. **Taigo Kato:** investigation, methodology, resources, validation, writing – review and editing. **Atsunari Kawashima:** investigation, methodology, resources, validation, writing – review and editing. **Takao Yamaguchi:** investigation, methodology, resources, validation, writing – review and editing. **Satoshi Obika:** investigation, methodology, supervision, validation, writing – review and editing. **Kosuke Yusa:** investigation, methodology, supervision, validation, writing – review and editing. **Norio Nonomura:** investigation, methodology, resources, supervision, validation, writing – review and editing. **Keisuke Nimura:** conceptualization, data curation, formal analysis, investigation, methodology, supervision, validation, writing – review and editing.

Acknowledgments

We thank Editage (http://www.editage.com) for the English language editing.

Ethics Statement

This study was approved by the Ethics Committee of Osaka University (No. 13397-23). All experimental procedures were conducted in accordance with the institutional and national ethical guidelines. *Animal studies*: No. 05-068-003.

Consent

In this study, written informed consent was obtained from all participants.

Conflicts of Interest

Norio Nonomura is an editorial board member of *Cancer Science*. The authors declare no conflicts of interest.

References

1. K. Hatano and N. Nonomura, "Systemic Therapies for Metastatic Castration-Resistant Prostate Cancer: An Updated Review," *World Journal of Men's Health* 41 (2023): 769–784.

2. S. P. Pitroda, I. M. Pashtan, H. L. Logan, et al., "DNA Repair Pathway Gene Expression Score Correlates With Repair Proficiency and Tumor Sensitivity to Chemotherapy," *Science Translational Medicine* 6 (2014): 229ra242.

3. K. Hatano and N. Nonomura, "Genomic Profiling of Prostate Cancer: An Updated Review," *World Journal of Men's Health* 40 (2022): 368–379.

4. C. C. Pritchard, J. Mateo, M. F. Walsh, et al., "Inherited DNA-Repair Gene Mutations in Men With Metastatic Prostate Cancer," *New England Journal of Medicine* 375 (2016): 443–453.

5. J. H. Chung, N. Dewal, E. Sokol, et al., "Prospective Comprehensive Genomic Profiling of Primary and Metastatic Prostate Tumors," *JCO Precision Oncology* 3 (2019): PO.18.00283.

6. R. J. Scott, A. Mehta, G. S. Macedo, P. S. Borisov, R. Kanesvaran, and W. El Metnawy, "Genetic Testing for Homologous Recombination Repair (HRR) in Metastatic Castration-Resistant Prostate Cancer (mCRPC): Challenges and Solutions," *Oncotarget* 12 (2021): 1600–1614.

7. J. Murai, S. Y. Huang, B. B. Das, et al., "Trapping of PARP1 and PARP2 by Clinical PARP Inhibitors," *Cancer Research* 72 (2012): 5588–5599.

8. H. Farmer, N. McCabe, C. J. Lord, et al., "Targeting the DNA Repair Defect in BRCA Mutant Cells as a Therapeutic Strategy," *Nature* 434 (2005): 917–921.

9. H. E. Bryant, N. Schultz, H. D. Thomas, et al., "Specific Killing of BRCA2-Deficient Tumours With Inhibitors of Poly(ADP-Ribose) Polymerase," *Nature* 434 (2005): 913–917.

10. J. Mateo, S. Carreira, S. Sandhu, et al., "DNA-Repair Defects and Olaparib in Metastatic Prostate Cancer," *New England Journal of Medicine* 373 (2015): 1697–1708.

11. J. Mateo, N. Porta, D. Bianchini, et al., "Olaparib in Patients With Metastatic Castration-Resistant Prostate Cancer With DNA Repair Gene Aberrations (TOPARP-B): A Multicentre, Open-Label, Randomised, Phase 2 Trial," *Lancet Oncology* 21 (2020): 162–174.

12. J. de Bono, J. Mateo, K. Fizazi, et al., "Olaparib for Metastatic Castration-Resistant Prostate Cancer," *New England Journal of Medicine* 382 (2020): 2091–2102.

13. W. Abida, A. Patnaik, D. Campbell, et al., "Rucaparib in Men With Metastatic Castration-Resistant Prostate Cancer Harboring a BRCA1 or BRCA2 Gene Alteration," *Journal of Clinical Oncology* 38 (2020): 3763–3772.

14. K. Fizazi, J. M. Piulats, M. N. Reaume, et al., "Rucaparib or Physician's Choice in Metastatic Prostate Cancer," *New England Journal of Medicine* 388 (2023): 719–732.

15. F. Saad, N. W. Clarke, M. Oya, et al., "Olaparib Plus Abiraterone Versus Placebo Plus Abiraterone in Metastatic Castration-Resistant Prostate Cancer (PROpel): Final Prespecified Overall Survival Results of a Randomised, Double-Blind, Phase 3 Trial," *Lancet Oncology* 24 (2023): 1094–1108.

16. N. Agarwal, A. A. Azad, J. Carles, et al., "Talazoparib Plus Enzalutamide in Men With First-Line Metastatic Castration-Resistant Prostate Cancer (TALAPRO-2): A Randomised, Placebo-Controlled, Phase 3 Trial," *Lancet* 402 (2023): 291–303.

17. T. Tsujino, T. Takai, K. Hinohara, et al., "CRISPR Screens Reveal Genetic Determinants of PARP Inhibitor Sensitivity and Resistance in Prostate Cancer," *Nature Communications* 14 (2023): 252.

18. A. Vaitsiankova, K. Burdova, M. Sobol, et al., "PARP Inhibition Impedes the Maturation of Nascent DNA Strands During DNA Replication," *Nature Structural & Molecular Biology* 29 (2022): 329–338.

19. M. Zimmermann, O. Murina, M. A. M. Reijns, et al., "CRISPR Screens Identify Genomic Ribonucleotides as a Source of PARP-Trapping Lesions," *Nature* 559 (2018): 285–289.

20. G. Hewitt, V. Borel, S. Segura-Bayona, et al., "Defective ALC1 Nucleosome Remodeling Confers PARPi Sensitization and Synthetic Lethality With HRD," *Molecular Cell* 81 (2021): 767–783.e1.

21. G. Fracassi, F. Lorenzin, F. Orlando, et al., "CRISPR/Cas9 Screens Identify LIG1 as a Sensitizer of PARP Inhibitors in Castration-Resistant Prostate Cancer," *Journal of Clinical Investigation* 135 (2024): e179393.

22. K. Tzelepis, H. Koike-Yusa, E. De Braekeleer, et al., "A CRISPR Dropout Screen Identifies Genetic Vulnerabilities and Therapeutic Targets in Acute Myeloid Leukemia," *Cell Reports* 17 (2016): 1193–1205.

23. W. Li, H. Xu, T. Xiao, et al., "MAGeCK Enables Robust Identification of Essential Genes From Genome-Scale CRISPR/Cas9 Knockout Screens," *Genome Biology* 15 (2014): 554.

24. P. L. Olive and J. P. Banáth, "The Comet Assay: A Method to Measure DNA Damage in Individual Cells," *Nature Protocols* 1 (2006): 23–29.

25. B. M. Gyori, G. Venkatachalam, P. S. Thiagarajan, D. Hsu, and M. V. Clement, "OpenComet: An Automated Tool for Comet Assay Image Analysis," *Redox Biology* 2 (2014): 457–465.

26. A. Ianevski, A. K. Giri, and T. Aittokallio, "SynergyFinder 3.0: An Interactive Analysis and Consensus Interpretation of Multi-Drug Synergies Across Multiple Samples," *Nucleic Acids Research* 50 (2022): W739–w743.

27. A. E. Tomkinson, S. Vijayakumar, J. M. Pascal, and T. Ellenberger, "DNA Ligases: Structure, Reaction Mechanism, and Function," *Chemical Reviews* 106 (2006): 687–699.

28. T. Ellenberger and A. E. Tomkinson, "Eukaryotic DNA Ligases: Structural and Functional Insights," *Annual Review of Biochemistry* 77 (2008): 313–338.

29. A. E. Tomkinson and D. S. Levin, "Mammalian DNA Ligases," *BioEssays* 19 (1997): 893–901.

30. D. Sun, R. Urrabaz, M. Nguyen, et al., "Elevated Expression of DNA Ligase I in Human Cancers," *Clinical Cancer Research* 7 (2001): 4143–4148.

31. T. R. L. Howes, A. Sallmyr, R. Brooks, et al., "Structure-Activity Relationships Among DNA Ligase Inhibitors: Characterization of a Selective Uncompetitive DNA Ligase I Inhibitor," *DNA Repair (Amst)* 60 (2017): 29–39.

32. X. Chen, S. Zhong, X. Zhu, et al., "Rational Design of Human DNA Ligase Inhibitors That Target Cellular DNA Replication and Repair," *Cancer Research* 68 (2008): 3169–3177.

33. A. K. Taylor, D. Kosoff, H. Emamekhoo, J. M. Lang, and C. E. Kyriakopoulos, "PARP Inhibitors in Metastatic Prostate Cancer," *Frontiers in Oncology* 13 (2023): 1159557.

34. C. Pezaro, "PARP Inhibitor Combinations in Prostate Cancer," *Therapeutic Advances in Medical Oncology* 12 (2020): 1758835919897537.

35. M. Asim, F. Tarish, H. I. Zecchini, et al., "Synthetic Lethality Between Androgen Receptor Signalling and the PARP Pathway in Prostate Cancer," *Nature Communications* 8 (2017): 374.

36. J. Chou, T. M. Robinson, E. A. Egusa, et al., "Synthetic Lethal Targeting of CDK12-Deficient Prostate Cancer With PARP Inhibitors," *Clinical Cancer Research* 30 (2024): 5445–5458.

37. J. Ma, Y. Zhou, P. Pan, et al., "TRABID Overexpression Enables Synthetic Lethality to PARP Inhibitor via Prolonging 53BP1 Retention at Double-Strand Breaks," *Nature Communications* 14 (2023): 1810.

38. G. E. Feiersinger, K. Trattnig, P. D. Leitner, et al., "Olaparib Is Effective in Combination With, and as Maintenance Therapy After, First-Line Endocrine Therapy in Prostate Cancer Cells," *Molecular Oncology* 12 (2018): 561–576.

39. K. Jamal, A. Galbiati, J. Armenia, et al., "Drug-Gene Interaction Screens Coupled to Tumor Data Analyses Identify the Most Clinically Relevant Cancer Vulnerabilities Driving Sensitivity to PARP Inhibition," *Cancer Research Communications* 2 (2022): 1244–1254.

40. A. Serrano-Benitez, S. E. Wells, L. Drummond-Clarke, et al., "Unrepaired Base Excision Repair Intermediates in Template DNA Strands Trigger Replication Fork Collapse and PARP Inhibitor Sensitivity," *EMBO Journal* 42 (2023): e113190.

41. A. E. Tomkinson, T. Naila, and S. Khattri Bhandari, "Altered DNA Ligase Activity in Human Disease," *Mutagenesis* 35 (2020): 51–60.

42. A. M. Sriramachandran, G. Petrosino, M. Méndez-Lago, et al., "Genome-Wide Nucleotide-Resolution Mapping of DNA Replication Patterns, Single-Strand Breaks, and Lesions by GLOE-Seq," *Molecular Cell* 78 (2020): 975–985.e7.

43. S. Kumamoto, A. Nishiyama, Y. Chiba, et al., "HPF1-Dependent PARP Activation Promotes LIG3-XRCC1-Mediated Backup Pathway of Okazaki Fragment Ligation," *Nucleic Acids Research* 49 (2021): 5003–5016.

44. S. F. El-Khamisy, M. Masutani, H. Suzuki, and K. W. Caldecott, "A Requirement for PARP-1 for the Assembly or Stability of XRCC1 Nuclear Foci at Sites of Oxidative DNA Damage," *Nucleic Acids Research* 31 (2003): 5526–5533.

45. H. Hanzlikova, W. Gittens, K. Krejcikova, Z. Zeng, and K. W. Caldecott, "Overlapping Roles for PARP1 and PARP2 in the Recruitment of Endogenous XRCC1 and PNKP Into Oxidized Chromatin," *Nucleic Acids Research* 45 (2017): 2546–2557.

46. K. Azarm and S. Smith, "Nuclear PARPs and Genome Integrity," *Genes & Development* 34 (2020): 285–301.

47. L. Li, S. Karanika, G. Yang, et al., "Androgen Receptor Inhibitor-Induced "BRCAness" and PARP Inhibition Are Synthetically Lethal for Castration-Resistant Prostate Cancer," *Science Signaling* 10 (2017): eaam7479.

48. R. Ali, M. Alabdullah, M. Algethami, et al., "Ligase 1 Is a Predictor of Platinum Resistance and Its Blockade Is Synthetically Lethal in XRCC1 Deficient Epithelial Ovarian Cancers," *Theranostics* 11 (2021): 8350–8361.

49. Y. C. Lee, H. Morgenstern, S. Greenland, et al., "A Case-Control Study of the Association of the Polymorphisms and Haplotypes of DNA Ligase I With Lung and Upper-Aerodigestive-Tract Cancers," *International Journal of Cancer* 122 (2008): 1630–1638.

50. S. Michiels, P. Danoy, P. Dessen, et al., "Polymorphism Discovery in 62 DNA Repair Genes and Haplotype Associations With Risks for Lung and Head and Neck Cancers," *Carcinogenesis* 28 (2007): 1731–1739.

51. H. Hanzlikova, I. Kalasova, A. A. Demin, L. E. Pennicott, Z. Cihlarova, and K. W. Caldecott, "The Importance of Poly(ADP-Ribose) Polymerase as a Sensor of Unligated Okazaki Fragments During DNA Replication," *Molecular Cell* 71 (2018): 319–331.e3.

Supporting Information

Additional supporting information can be found online in the Supporting Information section. **Figure S1:** Gene ontology and pathway analysis. (A) Gene ontology and pathway analysis of the top 200 drop-off genes in olaparib-treatment. (B) Gene ontology and pathway analysis of the top 200 enriched genes in olaparib-treatment. **Figure S2:** Evaluation of cell proliferation in *LIG1* or *TP53* knockout cells by MTS assay. **Table S1:** Negatively selected genes enhancing sensitivity to olaparib identified by genome-wide CRISPR-Cas9 knockout screening in 22Rv1. **Table S2:** Negatively selected genes enhancing sensitivity to olaparib identified by genome-wide CRISPR-Cas9 knockout screening in DU145. **Table S3:** Negatively selected genes enhancing sensitivity to olaparib identified by genome-wide CRISPR-Cas9 knockout screening in LNCaP. **Table S4:** Positively selected genes conferring resistance to olaparib identified by genome-wide CRISPR-Cas9 knockout screening in 22Rv1. **Table S5:** Positively selected genes conferring resistance to olaparib identified by genome-wide CRISPR-Cas9 knockout screening in DU145. **Table S6:** Positively selected genes conferring resistance to olaparib identified by genome-wide CRISPR-Cas9 knockout screening in LNCaP.